Neutron-induced fission cross section of ^{237}Np in the keV to MeV range at the CERN n_TOF facility

M. Diakaki,[1,2,*] D. Karadimos,[2] R. Vlastou,[2] M. Kokkoris,[2] P. Demetriou,[3] E. Skordis,[4,2] A. Tsinganis,[4,2] U. Abbondanno,[5] G. Aerts,[1] H. Álvarez,[6] F. Alvarez-Velarde,[7] S. Andriamonje,[1] J. Andrzejewski,[8] P. Assimakopoulos,[9,†] L. Audouin,[10] G. Badurek,[11] P. Baumann,[12] F. Bečvář,[13] E. Berthoumieux,[1] M. Calviani,[4] F. Calviño,[14] D. Cano-Ott,[7] R. Capote,[3] A. Carrillo de Albornoz,[15] P. Cennini,[4] V. Chepel,[16] E. Chiaveri,[4] N. Colonna,[17] G. Cortes,[14] A. Couture,[18] J. Cox,[18] S. David,[10] R. Dolfini,[19] C. Domingo-Pardo,[20] A. Dorochenko,[21] W. Dridi,[22] I. Duran,[6] Ch. Eleftheriadis,[23] M. Embid-Segura,[7] L. Ferrant,[10,‡] A. Ferrari,[4] R. Ferreira-Marques,[16] L. Fitzpatrick,[4] H. Frais-Koelbl,[24] K. Fuji,[17] W. Furman,[25] I. Goncalves,[15] R. Gallino,[26] E. Gonzalez-Romero,[7] A. Goverdovski,[21] F. Gramegna,[27] E. Griesmayer,[24] C. Guerrero,[7] F. Gunsing,[22] B. Haas,[28] R. Haight,[29] M. Heil,[30] A. Herrera-Martinez,[4] M. Igashira,[31] K. Ioannidis,[9] S. Isaev,[10] E. Jericha,[32] Y. Kadi,[4] F. Käppeler,[30] D. Karamanis,[9] M. Kerveno,[12] V. Ketlerov,[21] P. Koehler,[33] D. Kolokolov,[21] V. Konovalov,[25] M. Krtička,[13] C. Lamboudis,[23] H. Leeb,[32] A. Lindote,[16] I. Lopes,[16] M. Lozano,[34] S. Lukic,[12] J. Marganiec,[8] L. Marques,[15] S. Marrone,[17] C. Massimi,[35] P. Mastinu,[27] A. Mengoni,[4] P. M. Milazzo,[5] C. Moreau,[5] M. Mosconi,[30] F. Neves,[16] H. Oberhummer,[11] S. O'Brien,[18] M. Oshima,[36] J. Pancin,[22] C. Papadopoulos,[2] C. Paradela,[6] N. Patronis,[9] A. Pavlik,[11] P. Pavlopoulos,[37] L. Perrot,[22] R. Plag,[30] A. Plompen,[38] A. Plukis,[22] A. Poch,[14] C. Pretel,[14] J. Quesada,[34] T. Rauscher,[39] R. Reifarth,[29] M. Rosetti,[40] C. Rubbia,[19] G. Rudolf,[12] P. Rullhusen,[38] J. Salgado,[15] L. Sarchiapone,[4] I. Savvidis,[23] M. Sedysheva,[25] K. Stamoulis,[9] C. Stephan,[10] G. Tagliente,[17] J. L. Tain,[20] L. Tassan-Got,[10] L. Tavora,[15] R. Terlizzi,[17] G. Vannini,[35] P. Vaz,[15] A. Ventura,[41] D. Villamarin,[7] M. C. Vincente,[7] V. Vlachoudis,[4] F. Voss,[30] H. Wendler,[4] M. Wiescher,[18] and K. Wisshak[30]

(n_TOF Collaboration)

[1]*CEA/Saclay - DSM, Gif-sur-Yvette, France*
[2]*National Technical University of Athens, Athens, Greece*
[3]*Nuclear Data Section, International Atomic Energy Agency, A-1400 Vienna, Austria*
[4]*CERN, Geneva, Switzerland*
[5]*Istituto Nazionale di Fisica Nucleare, Trieste, Italy*
[6]*Universidade de Santiago de Compostela, Santiago de Compostela, Spain*
[7]*Centro de Investigaciones Energeticas Medioambientales y Technologicas, Madrid, Spain*
[8]*University of Lodz, Lodz, Poland*
[9]*University of Ioannina, Ioannina, Greece*
[10]*Centre National de la Recherche Scientifique/IN2P3 - IPN, Orsay, France*
[11]*Institut für Isotopenforschung und Kernphysik, Universität Wien, Vienna, Austria*
[12]*Centre National de la Recherche Scientifique/IN2P3 - IReS, Strasbourg, France*
[13]*Charles University, Prague, Czech Republic*
[14]*Universitat Politecnica de Catalunya, Barcelona, Spain*
[15]*Instituto Tecnológico e Nuclear, Lisbon, Portugal*
[16]*LIP - Coimbra and Departamento de Fisica da Universidade de Coimbra, Portugal*
[17]*Istituto Nazionale di Fisica Nucleare, Bari, Italy*
[18]*University of Notre Dame, Notre Dame, Indiana, USA*
[19]*Universita degli Studi Pavia, Pavia, Italy*
[20]*Consejo Superior de Investigaciones Cientificas - University of Valencia, Valencia, Spain*
[21]*Institute of Physics and Power Engineering, Kaluga region, Obninsk, Russia*
[22]*CEA/Saclay - DSM, Gifsur-Yvette, France*
[23]*Aristotle University of Thessaloniki, Thessaloniki, Greece*
[24]*Fachhochschule Wiener Neustadt, Wiener Neustadt, Austria*
[25]*Joint Institute for Nuclear Research, Frank Laboratory of Neutron Physics, Dubna, Russia*
[26]*Dipartimento di Fisica Generale, Universita di Torino and Sezione INFN di Torino, I-10125 Torino, Italy*
[27]*Istituto Nazionale di Fisica Nucleare, Laboratori Nazionali di Legnaro, Legnaro, Italy*
[28]*Centre National de la Recherche Scientifique/IN2P3 - CENBG, Bordeaux, France*
[29]*Los Alamos National Laboratory, Los Alamos, New Mexico, USA*
[30]*Karlsruhe Institut of Technology, Campus Nord, Institut für Kernphysik, Germany*
[31]*Tokyo Institute of Technology, Tokyo, Japan*
[32]*Atominstitut der Österreichischen Universitäten,Technische Universität Wien, Vienna, Austria*
[33]*Oak Ridge National Laboratory, Physics Division, Oak Ridge, Tennessee, USA*
[34]*Universidad de Sevilla, Sevilla, Spain*
[35]*Dipartimento di Fisica, Universita di Bologna, and Sezione INFN di Bologna, Italy*
[36]*Japan Atomic Energy Research Institute, Tokai-mura, Japan*
[37]*Pôle Universitaire Léonard de Vinci, Paris La Défense, France*
[38]*CEC-JRC-IRMM, Geel, Belgium*
[39]*Department of Physics and Astronomy, University of Basel, Basel, Switzerland*

[40]*ENEA, Bologna, Italy*
[41]*Istituto Nazionale di Fisica Nucleare, Bologna, Italy*
(Received 23 November 2015; revised manuscript received 12 January 2016; published 17 March 2016)

The neutron-induced fission cross section of ^{237}Np was experimentally determined at the high-resolution and high-intensity facility n_TOF, at CERN, in the energy range 100 keV to 9 MeV, using the ^{235}U(n,f) and ^{238}U(n,f) cross section standards below and above 2 MeV, respectively. A fast ionization chamber was used in order to detect the fission fragments from the reactions and the targets were characterized as far as their mass and homogeneity are concerned by means of α spectroscopy and Rutherford backscattering spectroscopy respectively. Theoretical calculations within the Hauser-Feshbach formalism have been performed, employing the EMPIRE code, and the model parameters were tuned in order to successfully reproduce the experimental fission cross-sectional data and simultaneously all the competing reaction channels.

DOI: 10.1103/PhysRevC.93.034614

I. INTRODUCTION

The study of neutron-induced reactions on minor actinides is of considerable importance in diverse fields of research, from fundamental to applied nuclear physics.

Fission is one of the most challenging and not well known phenomena in nuclear physics and, at present, an *ab initio* theory able to predict fission cross sections as well as the characteristics of the fission process does not exist. The theoretical investigation of the cross section for the fission channel is mainly based on phenomenological analyses with parameters that need to be tuned in order to reproduce the experimental data. Thus, highly accurate data are needed for the testing of the existing nuclear models and consequently for the improvement of their predictive power. Furthermore, the development of the new generation of the nuclear reactor technology, which aims at safer and cleaner energy production (generation IV: so-called fast reactors, partitioning and transmutation techniques, etc.), requires highly accurate cross-sectional data of all the neutron-induced reactions mainly on minor actinides. ^{237}Np is one of the priorities, because it is found in great abundance in spent nuclear reactor fuel and has a very long half-life ($\sim 10^6$ years). Therefore, the accurate determination of the cross section for all neutron-induced reactions on this isotope is of great importance in order to reduce the uncertainties in the design of the new systems, with fission being one of the dominant channels over a wide neutron energy range.

There are a number of cross-sectional data on the ^{237}Np(n,f) reaction in the international database EXFOR [1], most using ^{235}U(n,f) as reference [2–18], as well as ^{237}Np/^{235}U fission cross-sectional ratios [19–22]. However, these data exhibit discrepancies that reach 8%, mainly at the first and second chance fission plateaus. Furthermore, the evaluations ENDF/B-VII.1 [23], JENDL-4.0 [24], JEFF-3.2 [25], CENDL 3.1 [26], and ROSFOND-2010 [27] present differences of 3–4%. Such differences, although small, increase the uncertainties of the design of new reactor systems and limit the nuclear model predictive power. Accordingly, the remeasurement of this dataset is essential. The n_TOF Collaboration [28] aims at providing highly accurate data on neutron-induced reactions, mainly for the requirements of advanced nuclear technologies and nuclear astrophysics, using the CERN Neutron Time-of-Flight (n_TOF) facility. In this context, the fission cross-sectional measurements on actinides are an important part of these studies. In the present work, the measurement of the ^{237}Np(n,f) cross section with reference to the standard ^{235}U(n,f) and ^{238}U(n,f) cross sections was performed at n_TOF using a fast ionization chamber [29] in the energy range 0.1 to 9 MeV. Theoretical calculations of this cross section were carried out with the EMPIRE code (version 3.2) [30], within the Hauser-Feshbach formalism and with phenomenological models.

II. EXPERIMENTAL PROCEDURE

A. The n_TOF facility

The CERN n_TOF facility [31] is an innovative neutron source that combines unique features, such as high instantaneous flux, a neutron beam covering a wide energy range (from thermal to several hundreds of MeV), high resolution, and low background. The white neutron beam at n_TOF is produced via the spallation of protons with a momentum of 20 GeV/c on a thick lead target. The pulsed proton beam ($\sim 7 \times 10^{12}$ protons per pulse) is provided by the proton synchrotron (PS) accelerator complex of CERN, in the form of short pulses of 7 ns (1 σ) with a relatively low repetition rate ($\sim$0.25 Hz), thus avoiding the overlapping of two sequential neutron pulses, since the thermal neutrons reach the experimental area approximately 80 ms after the proton pulse hits the lead target. Furthermore, the high produced neutron flux within a small time interval limits the acquisition time and consequently maximizes the signal-to-background ratio.

The neutrons produced from the spallation cover a long flight path of 182.5 m in a vacuum tube before entering the experimental area. The neutron energies E are defined with the time-of-flight (TOF) technique. Thanks to the long flight path the facility presents an excellent neutron energy resolution, up to $\Delta E/E = 10^{-4}$ for thermal neutrons and 0.06 for neutrons with energies close to GeV. Before entering the experimental

*maria.diakaki@cea.fr
†Deceased.
‡Deceased.

Published by the American Physical Society under the terms of the Creative Commons Attribution 3.0 License. Further distribution of this work must maintain attribution to the author(s) and the published article's title, journal citation, and DOI.

area, the neutron beam is shaped by two collimators, the inner diameter of the second one varying, depending on the type of measurement performed: For fission cross-sectional measurements an inner diameter of 8 cm is used since the sample material is deposited on a large surface in order to allow for thin samples, associated with the smallest possible self-absorption of the fission fragments (FF). The contamination of the neutron beam with charged particles is minimized by a 1.5-T sweeping magnet. Shielding walls made of concrete and iron are severely reducing the background in the experimental area. The neutron beam line is extended for 12 m after the experimental area to the beam dump, made of polyethylene and cadmium in order to reduce the neutron backscattering. More details on the facility can be found in Refs. [31–33].

B. Fission detection setup

The fission detection setup used for the data analyzed in this work consisted of a fast ionization chamber (FIC) with fast timing properties, built for neutron-induced fission cross-sectional measurements on minor actinides at the n_TOF facility [29]. This detector was developed in collaboration between the Joint Institute of Nuclear Research (JINR), Dubna, the Institute of Physics and Power Engineering (IPPE), Obninsk (Russian Federation), and the Emerging Energy Technologies (EET) section of CERN. The detector consisted of a stack of cells each consisting of three electrodes. The central Al electrode, of 100-μm thickness, was actually the backing of the actinide targets and in most of the cases it was plated on both sides. The external electrodes, of 15-μm thickness, are used to define the electric field in the 0.5-cm-thick active gas-filled volume of the detector. The detector gas was Ar (90%)/CF_4 (10%), presenting high electron drift velocity. Since the detector was not working in proportional mode, gas circulation was not needed. The gas pressure was $\sim$720 mbar. As reported in Ref. [29], detailed Monte Carlo simulations showed that the attenuation factor in each detector cell, defined as the ratio of the transmitted neutron flux to the impinging neutron flux, is of the order of a few per thousand, with a total attenuation after 14 samples of less than 1%. Another important result is that the background induced by scattered neutrons in the materials of the detector is negligible. The distance between the spallation target and the first sample in the FIC detector was 185.4 m.

C. The targets

The detector chamber was housing a stack of 18 actinide samples, among them a ^{237}Np target and three ^{235}U and three ^{238}U reference targets, provided by the IPPE and the JINR. The actinide oxide targets were thin layers of 8 or 5 cm in diameter deposited on a 100-μm-thick Al backing with the painting technique. The ^{237}Np target and one from the ^{235}U and ^{238}U targets were characterized as far as the mass, thickness, and homogeneity are concerned. The experimental procedure, analysis, and results are described in detail in Refs. [2] and [34] and are briefly mentioned in the following paragraphs.

The total mass and isotopic impurities of the targets were determined via α spectroscopy. The activity of each target was measured with two Silicon Surface Barrier (SSB) detectors with different active surface areas. A small detector with 50 mm^2 was used in order to obtain good energy resolution, whereas a big detector with 3000 mm^2 was used for higher counting statistics. The solid angle between sample and detectors was determined with a calibrated ^{241}Am α source (uncertainty of 0.3%) complemented by numerical disk-to-disk solid angle calculations. The weighted average value was adopted as the final result, with uncertainties of less than 2%. The isotopic impurities of the targets were estimated with the same method and turned out to be negligible.

TABLE I. The FIC detector samples used in this work. The rest of the targets in the chamber are not reported here. All the targets except U5c are double sided and the total mass refers to the sum of the masses of the two sides of the target.

Isotope	Name	Total mass (mg)	Diameter (cm)	Position in detector
U-235	U5a	36.6 $\pm$ 0.7	8	4
U-238	U8b	26.3 $\pm$ 0.5	8	7
U-238	U8a	25.4 $\pm$ 0.3	8	8
Np-237	Np7	12.6 $\pm$ 0.2	8	9
U-235	U5b	12.79 $\pm$ 0.3	5	16
U-235	U5c	4.96 $\pm$ 0.06	5	17
U-238	U8c	18.93 $\pm$ 0.18	5	18

The properties of the targets are summarized in Table I. As already mentioned, for three of the targets the mass was experimentally determined, while for the rest of the targets the nominal mass values provided by the manufacturer were assumed, with an estimated uncertainty of 2%.

The actinide targets were examined as far as their thickness and homogeneity are concerned via Rutherford backscattering spectrometry (RBS) at the external ion-beam setup of the 5.5-MV HV TN-11 tandem accelerator of the Institute of Nuclear and Particle Physics at the N.C.S.R. "Demokritos," using a proton beam of 2 MeV. For each target 5–10 points were selected in order to check the homogeneity, and the spectra obtained were analyzed with SIMNRA v. 6.06 [35]. The targets turned out to be homogeneous within 10–15% (obtained from the standard deviation of the thickness of the points checked) and did not present any systematic trend, for example, less material at the edges or identical values at points of equal distance from the center of the target. This result, in combination with the smooth neutron beam profile, led to the conclusion that the effect of the target inhomogeneities on the final cross section results is negligible. The targets were additionally characterized for their homogeneity with the use of CR-39 detectors. The 10×10 cm^2 detectors were placed on top of the samples for exposure times of a few seconds to a few hours, depending on the activity of the sample, in order to achieve a surface-track concentration of at least 200 tracks/mm^2. The results were in good agreement with the RBS measurements, showing inhomogeneities of less than 17%.

III. DATA ACQUISITION AND ANALYSIS

Fission reactions were detected via the energy deposited in the gas by the fission fragments. The detector signals were digitized by means of flash analog to digital converters (FADC,

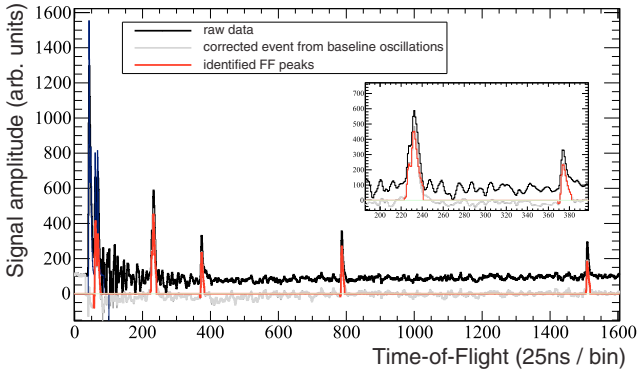

FIG. 1. Example of the analysis of a FADC event (black solid line). The corrected event from the baseline oscillations, after the subtraction of the appropriate fitted average event, is shown in gray. The fitted FF peaks are marked in red. The inset contains a zoom of the analysis in the bin region 200–400. Two peaks are successfully identified and fitted at the bins 220–240.

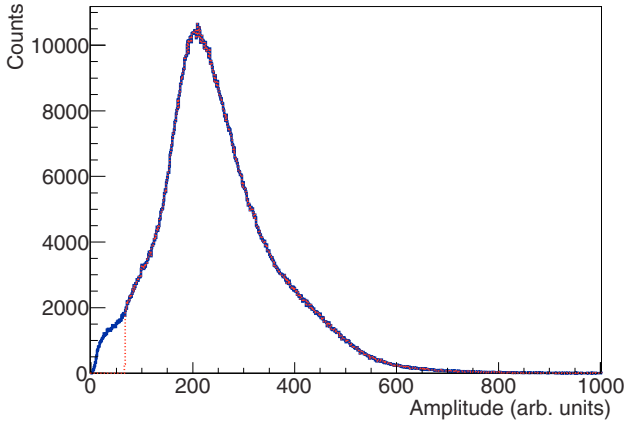

FIG. 2. The FF amplitude distribution from the pulse shape analysis of the ^{237}Np target. The blue curve corresponds to the analysis without additional threshold for the exclusion of low amplitude pulses, and the red dotted line corresponds to the amplitude distribution with the threshold chosen as discussed in Sec. III A.

LeCroy), with a sampling rate of 40 MHz. The FADC recorded the signal in a time window of 100 μs, which corresponds to neutron energies from GeV down to ~20 keV. The trigger signal for the start of the data acquisition is derived from a pickup in the proton beam line close to the lead target. The first signal to be recorded is the so-called γ flash produced by the impact of the proton pulse on the lead target. The γ flash consists of γ rays and relativistic particles from spallation processes in the target and of secondary particles produced in the experimental area. This signal serves for the accurate determination of the neutron time of flight. However, the large energy deposition of the γ flash causes malfunctions in the detector electronics, resulting in an undershooting of the signal baseline and intense rippling, especially for time bins in the early phase of the FADC event (bins ~50–400 in Fig. 1).

In view of these difficulties, a method based on pulse shape analysis techniques was developed for analyzing the FADC data in an automated way to provide a reliable background subtraction and identification of FF peaks even at high energies [36,37]. Starting from the observation that all the events follow the same baseline pattern in this region, an average FADC event ("average event") was produced for each detector channel by averaging many events starting from the time of the γ flash. This average event is free of FF peaks because they appear at random times. Due to the large number of bins available for the recording of the FIC signal, providing a time resolution of 25 ns, the possibility of having FF peaks that appear in the same time bin of the FADC event (i.e., the same time of flight) is indeed negligible.

For the analysis of individual events, the average event was fitted with a linear function in order to reproduce the baseline of the raw signal ("fitted average event"). Then, the fitted average event was subtracted from the event under analysis, thus removing the baseline oscillations. Then, the corrected event from baseline oscillations (Fig. 1) was checked, bin by bin, and if the threshold chosen is surpassed the code searches for local maxima until the background level chosen is reached. Then the FF peak candidates are fitted with Eq. (1) of Ref. [36], using the MINUIT code [38]. The γ-flash peak was fitted with the same function. Both the threshold and background levels are chosen by the user. A typical example of the signal analysis is given in Fig. 1. In order to have the average events as close as possible to the baseline of the raw data, the events were grouped into categories with similar γ-flash integral and an average event was extracted from each category. For the analysis of each event, the corresponding average event was chosen.

The baseline subtraction based on the average event gives the possibility to extract FF peaks even if they are very close to the γ flash, where the oscillations are severe. However, these oscillations caused signal saturations in some cases, especially in the neutron energy region above 9–10 MeV (i.e., for bins <200). This problem limited the neutron energy range of the present work to $E_n < 9$ MeV.

The parameters and errors from the fit of the average event, of the γ-flash peak, and of the FF peaks are stored in histograms for further selection. With this information, it is possible to reject events or FF peaks by reducing the parameter space for the γ flash, the average event, or the FF signals. For each target a separate analysis was performed to define the accepted limits of the fitting parameters and corresponding errors. In total, about 4×10^5 events were accepted per target, with a very small percentage of rejected events. A typical amplitude distribution of the accepted FF pulses from the analysis of ^{237}Np is shown in Fig. 2.

A. Sensitivity tests

The sensitivity of the results with respect to various procedures used in data analysis was examined to estimate possible systematic uncertainties. In the following, the low FF counting rate targets (U5c, U8c, U8a, U8b) correspond to the ones with low mass and/or low fission cross-sectional value at the so-called plateau (FADC bins below 400, i.e., neutron energies higher than ~2 MeV), and higher FF counting rate targets (Np7, U5b, U5a) correspond to targets with high mass and cross-sectional values in this energy region.

First, the events were grouped into categories with similar γ-flash integral and an average event was extracted from each group. Various categorizations were tried in order to find the best settings by checking the raw data and the reaction rate of each target. Due to the large similarity of the oscillation pattern after the γ flash, the reproduction of the baseline of the raw data by the fitted average events was found to be insensitive to the categorization chosen. Some differences in the early phase of the FADC event, where the frequency of the FFs is higher, were noticed in the reproduction of the baseline between the targets with low FF counting rate and those with higher FF counting rate. For the former, the reproduction of the baseline by the fitted average event was very good. In the case of the latter, the fitted average event often slightly overestimated the baseline in the bin region 300–700, the high FF counting rate in this region making the smoothing procedure more difficult. For these targets a coarser categorization was preferred because the reproduction of the baseline was improved (due to the better statistics in each category). However, the differences in the final reaction rates for different categorizations of the events did not exceed the corresponding statistical uncertainties in the whole neutron energy range examined, for all the targets.

Second, the sensitivity of the results on the choice of the threshold level chosen was examined. Various threshold values within reasonable limits were tried by checking the resulting amplitude distributions within the uncertainties of the fit parameters. It was shown that the results of the pulse shape analysis do not significantly change, although the differences were becoming larger at higher neutron energies where the oscillations of the raw data are stronger. But even in this case mainly the low amplitude pulses were affected and the final reaction rates varied only within 2–3% for all targets. By checking the effect of the different threshold values on the analysis of the raw data, the resulting pulse shape analysis parameters, and the corresponding uncertainties, a common threshold was chosen for the analysis for all the targets.

The choice of the background level determines the point at which the code quits looking for another local maximum and fits the peak(s) found. A study of the sensitivity of the results on this parameter was thus considered essential, especially for higher FF rate targets, where nonisolated peaks are more frequent. The effect of various background levels on the amplitude distribution of the FF peaks in the case of the Np7 target is illustrated in Fig. 3. Similar amplitude distributions were obtained for the other six targets. The differences are again mainly found in the low part of the FF distributions. Finally, an additional threshold was applied to exclude the residual low amplitude peaks which were sensitive to changes of the analysis parameters. This threshold was chosen to be at the minimum between the low amplitude peak and the main peak of the FF distribution with background level 0 (Fig. 3).

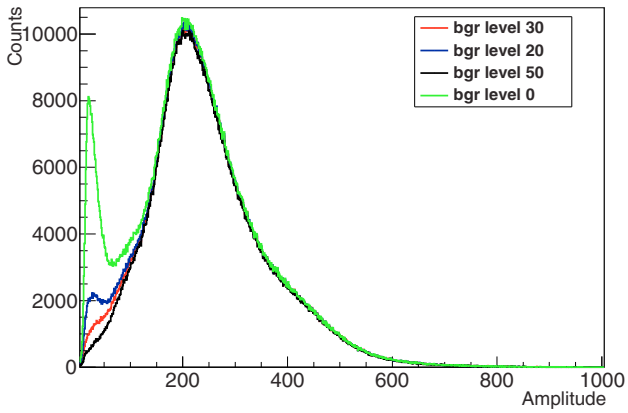

FIG. 3. The histograms of the FF amplitude distributions obtained with different choices of the background level, from the pulse shape analysis of the Np7 target data.

B. Cross-sectional calculation

The cross section $\sigma_{\rm tar}$ with reference to a standard fission cross section $\sigma_{\rm ref}$ is given by Eq. (1):

$$\sigma_{\rm tar} = \frac{C_{\rm tar} S_{\rm tar} A_{\rm tar} N_{\rm ref} \Phi_{\rm ref} \epsilon_{\rm ref}}{C_{\rm ref} S_{\rm ref} A_{\rm ref} N_{\rm tar} \Phi_{\rm tar} \epsilon_{\rm tar}} \sigma_{\rm ref}, \quad (1)$$

where C_i denotes the number of accepted FF peaks above the analysis threshold, S_i is the correction factors for the subthreshold FF counts (for the extrapolation below the additional analysis threshold chosen, see Fig. 2), N_i is the corresponding number of target nuclei, Φ_i is the total number of protons impinging on the spallation target used for normalization to equal neutron flux, and ϵ_i is the efficiency correction factor due to the loss of FFs in the sample. A_i is the neutron beam interception factor, and in fission measurements $A_{\rm tar}/A_{\rm ref}$ is equal to unity if the two targets are of equal diameter. The normalization to the number of protons, Φ_i, was introduced in order to account for the small difference in the number of accepted events between the targets. The systematic uncertainty induced by the $\Phi_{\rm ref}/\Phi_{\rm tar}$ factor was of the order of a few ‰, due to the very small percentage of rejected events, and thus was considered negligible.

The efficiency correction due to the self-absorption of the FFs in the samples as well as the percentage of the FF counts below the threshold were estimated via Monte Carlo simulations performed with the code FLUKA [39]. In the latest versions of FLUKA the stopping power models have been thoroughly reworked and are more precise, particularly for heavy ions: the Barkas (Z^3), Bloch (Z^4), and Mott corrections have been implemented, and the nuclear stopping power is calculated and taken into account. The geometry of each target cell and the respective target side thickness (determined in the RBS measurements, assuming the stoichiometry as NpO_2, U_3O_8) were properly considered. The generation of the FFs was performed with an external routine. The mass and charge distributions of the FFs for each isotope, as well as the total kinetic energy provided to both FFs (heavy and light) after the fission reaction, were determined from systematics of the actinide region [40,41]. The energy deposition of the FFs in the detector gas was subsequently scored.

The efficiency ϵ_i was calculated by the ratio of the FFs depositing energy in the gas to the total number of FFs generated. The results for all the targets are presented in Table II. The loss of FFs in the targets does not exceed 3.5% for the thicker one (U8c). Thanks to the high statistics of the simulations, the corresponding statistical uncertainty was less

TABLE II. The correction factors for the detection efficiency (ϵ_i) and the subthreshold FF counts (S_i), obtained with the FLUKA simulations.

Target name	ϵ_i	S_i
U5a	0.970	1.049
U8b	0.982	1.026
U8a	0.982	1.026
Np7	0.993	1.007
U5b	0.975	1.035
U5c	0.980	1.026
U8c	0.965	1.056

than ∼0.1% for the sum of heavy and light FFs, while the systematic uncertainty of these calculations was estimated to be about 2%.

The S_i correction was calculated from the simulated energy deposition histograms. In principle this requires the calibration of the experimental amplitude distributions, in order to find the energy corresponding to the bin of the threshold chosen in the analysis. The major difficulty in this case is that the amplitude distribution does not exhibit discrete heavy and light FF peaks as the simulated histograms, due to the nonproportionality of the detector and the electronic chain. Therefore, the experimental amplitude distribution was fitted with two Gaussian peaks, skewed with a tail towards lower amplitudes, as predicted by the simulations. Two spectra analysis programs were used for this fitting, SPECTRW [42] and TV [43], in order to check the sensitivity and to estimate the related systematic uncertainty. The reproduction of the experimental distribution with two Gaussians of equal area and different shape was satisfactory (integral values agreed within 1%), and the centroids of these Gaussians were used to calibrate the experimental amplitude distributions. The energies attributed to the thresholds chosen varied from 30 to 36 MeV for the different targets, thus excluding possible counts from α particles. The calculated correction factors for the subthreshold FF counts, S_i, can be found in Table II. The analyses with the two programs changed the energy attributed to the threshold chosen by less than 5 MeV. The resulting systematic uncertainty of the calculated S_{target} values depended on the quality of the fit and the thickness of the target and was less than 1% in the worst case (U8c). The corresponding statistical uncertainties were negligible.

As reference, the cross section of the $^{235}U(n,f)$ reaction was used up to 2 MeV and the $^{238}U(n,f)$ reaction up to 9 MeV. In order to validate the analysis procedure, the $^{238}U(n,f)$ cross section was calculated and compared to the recommended values in the neutron energy range where it is considered a standard. The cross section of the $^{238}U(n,f)$ reaction taking U8c as target and U5c and U5b as reference targets, is compared in Fig. 4 with the data from the ENDF/B VII-1 [23] evaluation. The present results generally agree with the ENDF evaluation, thus giving confidence on the normalization factors used.

However, the $^{238}U(n,f)$ cross-sectional data obtained with the big diameter targets, i.e., U8a, U8b, and U5a, slightly overestimated the evaluated cross sections for neutron energies

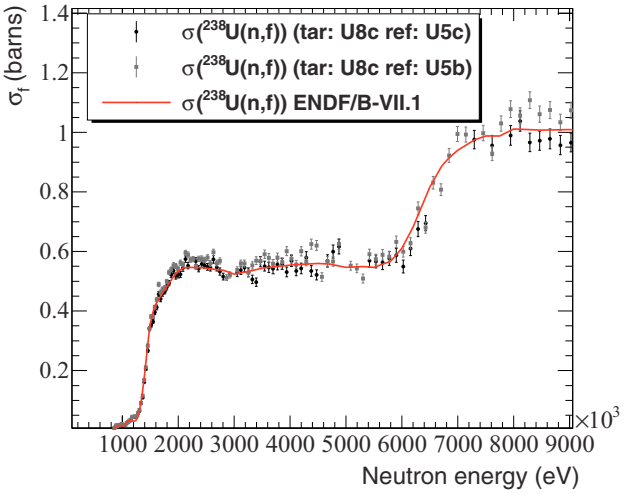

FIG. 4. The $^{238}U(n,f)$ cross section obtained with the small diameter targets: U8c as target and U5c (black points) and U5b as reference targets. The ENDF/B VII-1 [23] evaluation is shown for comparison. The results are given with a resolution of 50 bins / decade and the error bars correspond to the statistical uncertainties only.

in the energy range 0.6–4 MeV. It was found that this effect was due to loss of FF pulses in the analysis of the U5a target, which was by far the most massive. In this energy region both the $^{235}U(n,f)$ cross section and the n_TOF flux are large so that the FF peaks were not completely smeared out in the average event. The fitted average event thus overestimated the baseline of the corresponding event and consequently the shape of the FF pulses was in some cases deformed and not recognized by the routine. By checking on an event-by-event basis, the resulting losses never exceeded 3–3.5% in this neutron energy region, but depended on the neutron energy. In order to avoid such systematic uncertainties in the final cross-sectional values, it was decided to use the U5b as reference target for the cross section in this neutron energy range (400 keV to 2 MeV) because it has a FF rate very close to Np7.

Nevertheless, the Np7 (8 cm diameter) and the reference U5b target (5 cm diameter) have different surfaces, and thus A_{tar}/A_{ref} in Eq. (1) is not equal to unity, so the difference in the neutron beam flux had to be carefully taken into account. Monte Carlo simulations of the neutron beam profile of the n_TOF facility [44], assuming perfect alignment of the collimators, show that in the energy range 1 keV to 10 MeV the beam profile is practically stable with reference to the neutron beam and there is a small neutron fluence decrease at the edges of the 8-cm targets. Consequently, the ratio of the simulated fluence impinging on the surface of the 8-cm-diameter target is predicted to be ∼4% lower than the corresponding value for the 5-cm-diameter target. These fluence differences were determined experimentally, using the reaction rates and cross-sectional ratios with the low FF rate targets of different surfaces, as explained below.

(1) Reaction rate ratios ($\frac{RR_{8cm}}{RR_{5cm}}$) obtained from targets of the same isotope should be equal to unity. However, it

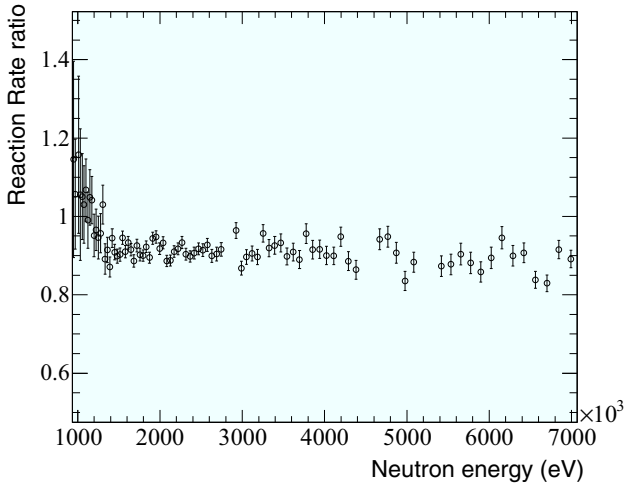

FIG. 5. The reaction rate ratio ($\frac{RR_{U8a}}{RR_{U8c}}$), plotted with 50 bins/decade.

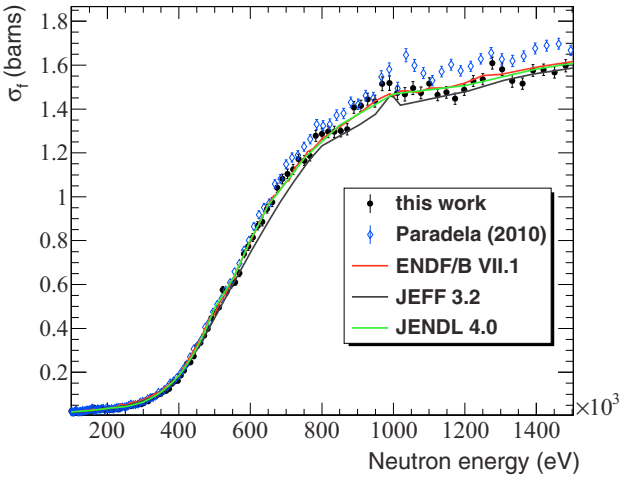

FIG. 6. The ^{237}Np(n,f) cross section, shown with 50 bins / decade, in the neutron energy range 100 keV to 1.5 MeV. The error bars correspond to the statistical uncertainties. The relative statistical uncertainty did not exceed 3% above 500 keV. The present results are compared to the latest experimental data of Paradela [3] (obtained from the same facility) and to the evaluations ENDF/B-VII.1 [23], JEFF 3.2 [25], and JENDL 4.0 [24].

was found that such reaction rate ratios from different target combinations were lower than unity by a constant factor. An example is shown in Fig. 5, for the reaction rate ratio $\frac{RR_{U8a}}{RR_{U8c}}$. The reaction rate ratios of the U5 targets were also taken into account, in the energy range 1 keV to 400 keV, where no loss of FF pulses was observed. By fitting experimental reaction rate ratios with a linear function in energy ranges below 5 MeV, the weighted average offset value of the fitting was $b_{RR} = 0.905 \pm 0.015$ while the corresponding slope was of the order of 10^{-9} to 10^{-10} eV^{-1}. Thus the effective neutron fluence correction was $A_{\rm tar}/A_{\rm ref} = 1/b_{RR} = 1.10 \pm 0.02$.

(2) ^{238}U(n,f) cross section ratios ($\frac{\sigma_{exp}}{\sigma_{ENDF}}$), where σ_{exp} corresponds to the experimental ^{238}U(n,f) cross section measured with a 8-cm-diameter ^{238}U target and a 5-cm-diameter ^{235}U reference target, and σ_{ENDF} to the corresponding ENDF/B VII-1 [23] evaluation, should also be equal to unity. However, also in this case, the experimental cross-sectional ratio was lower than unity by a constant factor. Two cross-sectional ratios were used (U8a and U8b as targets, and U5c as reference) and by fitting with a linear function in energy ranges below 5 MeV, the resulting average offset value was $b_{CS} = 0.91 \pm 0.02$ (the uncertainty corresponds to the fitting parameter error which was larger than the standard deviation of the various offsets obtained in the present case), in very good agreement with the b_{RR}. The effective neutron fluence correction also in this case was $A_{\rm tar}/A_{\rm ref} = 1/b_{CS} = 1.10 \pm 0.02$.

The final adopted value of the correction for the effective neutron fluence in the neutron energy range of interest was 1.10, with an estimated uncertainty of 1.7%. This value was obtained from ratios of different targets, thus possible small systematic uncertainties from the mass values and/or inhomogeneities are assumed to cancel out.

IV. RESULTS AND DISCUSSION

The final cross section values of the ^{237}Np(n,f) reaction were determined as follows:

(i) neutron energy range 100–400 keV: The U5a sample was used as reference target in this neutron energy region, since it yields good statistics in a TOF region where the raw data analysis is not problematic, and it is of the same diameter as Np7. It has to be noted that also when the U5b and U5c targets are used as reference, the cross-sectional results were found to agree within statistical uncertainties, giving more confidence on the analysis procedure and the normalization factors used (masses, efficiencies etc).

(ii) neutron energy range 400 keV to 2 MeV: The U5b target was used as a reference in this energy region, using Eq. (1) and considering the correction factor for the difference in the effective neutron fluence.

(iii) neutron energy range above 2 MeV: The U8a and U8b targets were used as a reference in this energy region. Two cross-sectional sets were calculated and the average was adopted as the final result. Consistent results were obtained with the U5b and the U5c targets as reference; however, the U8a and U8b targets were preferred in this energy region mainly because they have the same diameter as the Np7 target so no effective neutron fluence correction factor was needed.

The final ^{237}Np(n,f) cross-sectional values are presented in Figs. 6 and 7, along with the latest data of Paradela (obtained from the same facility) [3] and Diakaki [2] (obtained with the same ^{237}Np target), and the latest evaluated datasets, ENDF/B-VII.1 [23], JEFF 3.2 [25], and JENDL 4.0 [24]. The data are presented with 50 bins/decade and only the

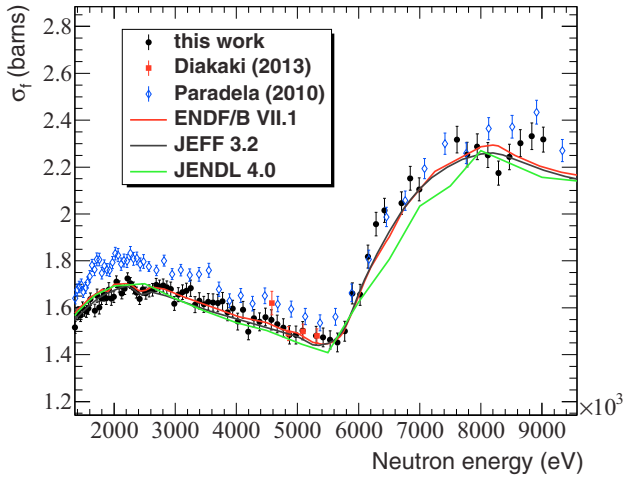

FIG. 7. The ^{237}Np(n,f) cross section, shown with 50 bins/decade, in the neutron energy range 1.5–9 MeV. The error bars correspond to the statistical uncertainties. The present data are compared to the experimental data of Paradela [3] (obtained from the same facility) and Diakaki [2] (obtained with the same target at another neutron production facility as explained in the text), and the evaluations ENDF/B-VII.1 [23], JEFF 3.2 [25], and JENDL 4.0 [24].

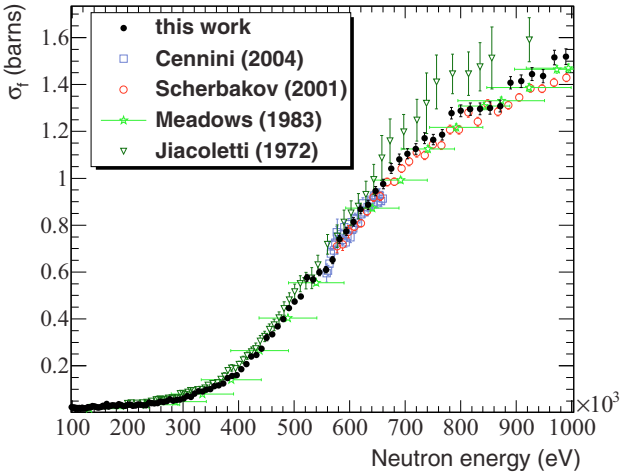

FIG. 8. Comparison of the present data with selected data from the EXFOR database [1], in the neutron energy range 100 keV to 1 MeV.

statistical uncertainties are shown in the figures. The few bins containing data at energies of saturations have been removed. A summary of the estimated systematic uncertainties of the correction factors of the cross section calculation can be found in Table III.

The data obtained from this work agree within errors with the latest data of Ref. [3] and the latest ENDF and JENDL evaluations up to 1 MeV (Fig. 6), while the latest JEFF evaluation is systematically slightly lower in the range 600 keV to 1 MeV. The cross section presents local maxima at ∼1 and ∼1.3 MeV, which appear also in the data of Ref. [3], but only the first feature appears in the shape of the JEFF evaluation. In the energy range 1–6 MeV the data from the present work are somewhat systematically lower than the data of Ref. [3], although in most of the cases the two datasets agree within their combined uncertainties, and they agree within errors with the latest evaluations. Further measurements have been performed using the same ^{237}Np target as described in Ref. [2] and the results are shown for comparison in Fig. 7. These measurements were performed with monoenergetic neutron beams and using a Micromegas detector, at the Institute of Nuclear and Particle Physics at the N.C.S.R. "Demokritos", within the context of the n_TOF collaboration. The data points from this measurement are in good agreement with the present cross-sectional set, giving confidence about the reliability of the obtained results. From 6 to 9 MeV, at the threshold of the second-chance fission, the present data agree within errors with the data of Ref. [3] and the latest evaluations.

For completeness, a comparison with selected experimental datasets is shown in Figs. 8, 9, and 10. The present data agree within errors with the data of Cennini [5] at the threshold of the first-chance fission; generally agree with the dataset of Shcherbakov [4] (although at the second-chance fission threshold the latter data are somewhat lower) and the datasets of Lisowski [7] and Meadows [10]; and generally present significant differences with those of Jiacoletti [13]. The dataset

TABLE III. Systematic uncertainties of the correction factors used in the cross-sectional calculation. The third column contains the energy range in which these uncertainties contribute to the cross-sectional results.

Source of uncertainty	Uncertainty (%)	Energy range (MeV)
Target mass	1.6–2 %	0.1–9
Threshold correction	<0.5%	0.1–9
Efficiency correction	2%	0.1–9
Neutron fluence correction	1.7%	0.4–2
$\sigma_{^{235}U(n,f)}$	<1%	0.1–2
$\sigma_{^{238}U(n,f)}$	<1%	2–9

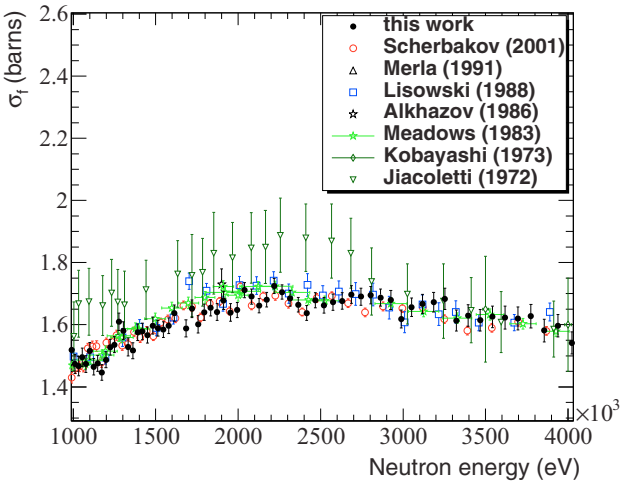

FIG. 9. Comparison of the present data with selected data from the EXFOR database [1], in the neutron energy range 1–4 MeV.

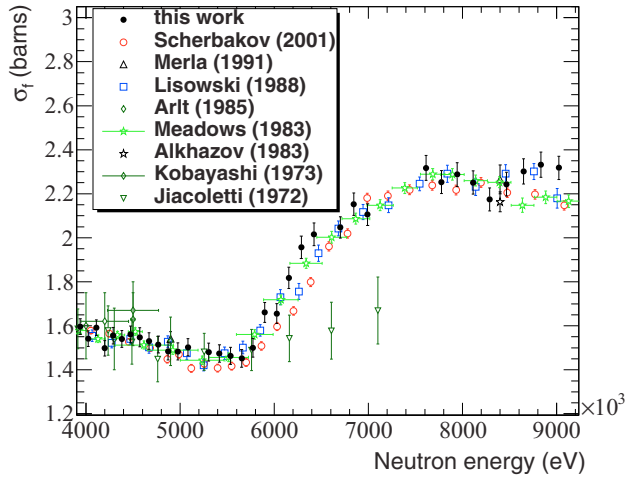

FIG. 10. Comparison of the present data with selected data from the EXFOR database [1], in the neutron energy range 4–9 MeV.

of Plattard (1975) [1] was not plotted for clarity reasons, because the data points are very dense, but it has to be noted that it agrees with the present dataset up to 1 MeV and is systematically higher above that energy (up to 2 MeV).

V. NUCLEAR MODEL CALCULATIONS

Nuclear model calculations were performed in an effort to reproduce the experimentally obtained cross-sectional values with the code EMPIRE [45]. EMPIRE is a widely used modular system of nuclear reaction codes, comprising various nuclear models and designed for nuclear reaction calculations over a wide energy range and incident particle and target combinations, and it can be used for theoretical calculations as well as for nuclear data evaluation. The code accounts for the major nuclear reaction models, such as the optical model (for fission as well), coupled channels, DWBA, multistep direct, multistep compound, pre-equilibrium exciton model, and the full Hauser-Feshbach model with γ cascade including width fluctuations for the compound nucleus decay. In the present study the latest version of EMPIRE was used (version 3.2 [30]). The fission formalism implemented in EMPIRE has been continuously updated by incorporating fundamental features of the fission process and it has been shown that it can reproduce neutron-induced cross sections on light actinides [46,47]. The optical model for fission considers the transmission mechanisms through multihumped fission barriers using a complex optical potential ($V_f = V + iW$). The real part of the barriers V is parametrized by smoothly joined parabolas as a function of the deformation β. The parabolas are defined by maxima B_i (humps) and minima $B_{I,II}$ (wells) and their curvature $\hbar\omega$. The discrete transition states are rotational levels built on vibrational or noncollective band heads with given angular momentum J, parity π, and angular momentum projection on the nuclear symmetry axis K. For each transition state, there is a parabolic barrier associated with it. The negative imaginary potential iW is associated with the discrete vibrational states built on top of the wells. For a double-humped barrier there is only one well B_{II} and the imaginary potential is introduced to simulate damping of the class II vibrational states in this second well, causing absorption of the incoming flux. In this version of the model, partial damping of these states is assumed only. More details on the optical model for fission can be found in Refs. [48,49]. The EMPIRE code considers all competing nuclear reaction mechanisms in the energy range from 1 keV to 20 MeV. Compound nucleus decay through multiparticle emission and fission is calculated with the statistical Hauser-Feshbach (HF) [50] and Hofmann-Richert-Tepel-Weidenmueller (HRTW) models [51]. Direct interactions and transmission coefficients for the incident and outgoing channels are obtained from the dispersive coupled-channel deformed optical model of Ref. [52] using the coupled-channels code ECIS06 [53]. The fission channel is treated within the optical model for fission as described above. Pre-equilibrium emission is calculated with the exciton PCROSS model [45]. Nuclear level densities for ground-state and saddle-point deformations are obtained from the Empire global specific model [45], which is based on the enhanced generalized superfluid model [54] (including adjustments to discrete levels). Discrete levels were taken from the RIPL-3 level file [55]. The empirical fission barriers and fission transitions states of Maslov [55] were used initially for all nuclei considered in the calculations. Using the default values of the parameters in the models mentioned in the previous paragraph, we obtain total, inelastic, fission, and $(n, 2n)$ cross sections for incident neutrons on ^{237}Np.

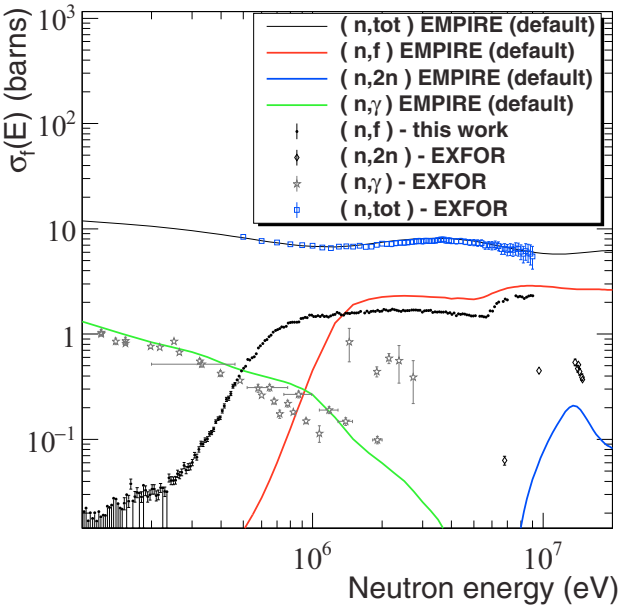

FIG. 11. The calculated cross sections for the main neutron-induced reaction channels of ^{237}Np, with the code EMPIRE and the default parameters of the models chosen, in the energy range 100 keV to 20 MeV, along with the corresponding experimental data from the EXFOR database [1]. The results for the (n,tot), (n,γ), (n,f), and $(n,2n)$ reaction channels are shown, the latter two exhibiting significant differences compared to the experimental data.

In Fig. 11 the calculated cross sections are compared with existing data for the above mentioned channels. Since no data exist for the inelastic channel these cross sections are omitted

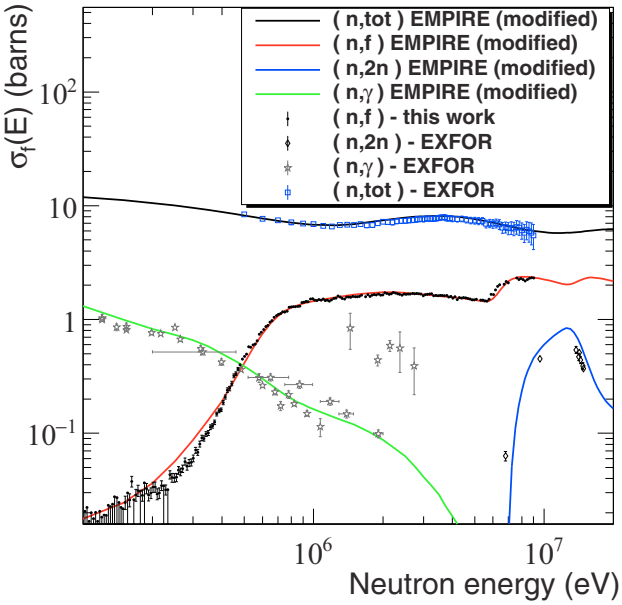

FIG. 12. The calculated cross-sectional results for the main neutron-induced reaction channels on ^{237}Np, with the code EMPIRE and modified parameters as explained in the text, in the energy range 100 keV to 20 MeV, along with the corresponding experimental data found in the EXFOR database [1]. A good agreement with the experimental data was obtained.

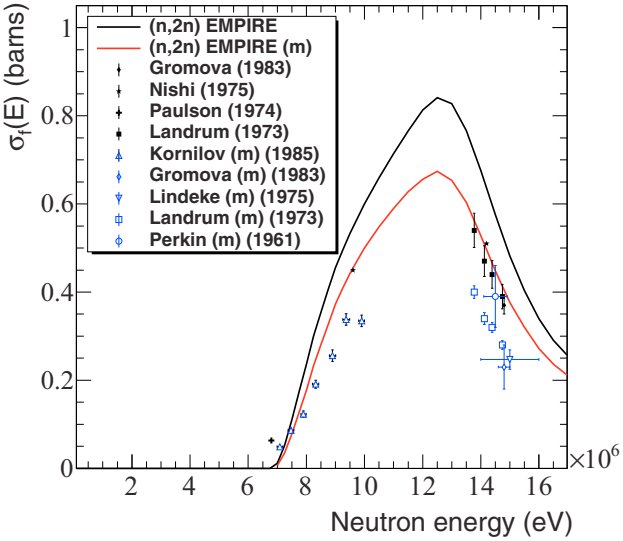

FIG. 13. The calculated cross-sectional results for the ^{237}Np$(n,2n)$ reaction with the code EMPIRE and modified parameters as explained in the text. The black line corresponds to the calculated total ^{237}Np$(n,2n)$ ^{236}Np reaction and the red line to the ^{237}Np$(n,2n)$ ^{236m}Np reaction that leads to the formation of the 22.5-h isomeric state. The corresponding data found in the EXFOR database [1] are also plotted for comparison, the black points representing the ^{237}Np$(n,2n)$ ^{236}Np reaction data and the blue points the ^{237}Np$(n,2n)$ ^{236m}Np reaction data.

from the figures. The total cross sections are reproduced well, which shows that the optical potential of Ref. [52] is suitable for this nucleus. The (n,f) and $(n,2n)$ channels, on the other hand, show discrepancies between calculations and data. First-chance fission is seriously underestimated up to 1 MeV, while above 1 MeV it is overestimated. Also, the $(n,2n)$ cross section is underestimated and there is no calculation of the production cross section of the isomeric state of ^{236}Np. An attempt to improve the description of the data was made and the results are shown in Fig. 12. The fission cross section is nicely reproduced over the whole energy range that is herein considered. This was achieved by making adjustments in the empirical fission barrier parameters [55] for ^{238,237,236}Np that are summarized in Table IV.

At first sight, modifications of the order of 20–30% may seem rather large; however, considering that fission barriers are not directly measured quantities but their parameters are extracted indirectly from cross-section measurements and therefore depend on various model assumptions and other nuclear parameters such as the level densities, it is reasonable to expect that the extracted empirical values [55] are associated with large uncertainties.

In addition, the ratio $a_f/a_{g.s.}$ was set equal to one, for both ^{238}Np and ^{237}Np. The level densities at the saddle points were further rescaled to reproduce the first- and second-chance fission plateau. The number of transition and vibrational states over states taken into account on top of the barriers and in the second well was reduced to those with the smallest bandhead energies.

To improve the description of the ^{237}Np$(n,2n)$ ^{236}Np channel, the discrete level scheme of ^{236}Np provided in the RIPL-3 level file [55] was modified. First, the number of discrete levels in ^{236}Np was changed from $N_{\max} = 1$ to 5 to allow for more than one discrete levels of ^{236}Np to be read by the EMPIRE code. Thus, not only the long-lived isomer of 1.15×10^5 y but also the short-lived isomer with 22.5-h half-life could be included in the calculations. It was thus possible to obtain a cross section for the production of ^{236}Np in its metastable state for comparison with existing measurements. To further improve the ratio of isomeric to ground-state production of ^{236}Np in the $(n,2n)$ channel, the discrete level scheme in the RIPL-3 file was completely replaced with a level scheme using bandhead energies and spins from the model of Sood [56]. The

TABLE IV. Final fission barrier parameters and their corresponding adjustments compared to the empirical ones found in Ref. [55].

Isotope	B_1 (MeV)	$\hbar\omega_1$ (MeV)	B_2 (MeV)	$\hbar\omega_2$ (MeV)
^{238}Np	6.135 (↓ 6%)	0.455 (↓ 24 %)	5.85 (↑ 2 %)	0.450 (↑ 12 %)
^{237}Np	6.10 (↑ 2 %)	0.700 (↓ 30 %)	5.95 (↑ 10 %)	0.600 (↓ 20 %)
^{236}Np	5.40 (↓ 10 %)	0.600 (no change)	5.30 (↓ 2 %)	0.400 (no change)

results are shown in Fig. 13 where one can see that the relative contributions of the transitions to ground-state and metastable state are in agreement with the experimental data; however, the absolute magnitudes of these contributions are rather high and overestimate the experimental data. This overestimation may also result from the incorrect description of the competing second-chance fission and the $(n,2n)$ channels. Further work is required to resolve this issue, which is beyond the scope of this paper.

VI. CONCLUSIONS

The ^{237}Np(n,f) cross section was experimentally determined at the CERN n_TOF facility, in the neutron energy range 100 keV to 9 MeV, using a fast ionization chamber. The cross-sectional results were obtained relative to the ^{235}U(n,f) cross section up to 2 MeV and to the ^{238}U(n,f) cross section above, using data from the ENDF/B-VII.1 library. Both reference reactions are considered as standards in the corresponding energy range (the ENDF/B-VII.1 evaluation was used). The present results extend over an important energy range where some discrepancies were observed in previous data. They are in good agreement with data from measurements [2] taken with the same ^{237}Np target, using monoenergetic neutron beams at the N.C.S.R. "Demokritos" but with Micromegas detectors. Finally, a theoretical investigation of the ^{237}Np(n,f) reaction cross section within the Hauser-Feshbach formalism with the code EMPIRE was performed, in the energy range 100 keV to 20 MeV, by successfully reproducing simultaneously the cross section of the ^{237}Np$(n,$tot$)$ reaction and the other competing reaction channels in the corresponding energy region.

ACKNOWLEDGMENTS

This research has been cofinanced by the European Union (European Social Fund - ESF) and Greek national funds through the Operational Program "Education and Life-long Learning" of the National Strategic Reference Framework (NSRF) - Research Funding Program: Heracleitus II.

[1] N. Otuka *et al.*, Nucl. Data Sheets **120**, 272 (2015).
[2] M. Diakaki, M. Kokkoris, A. Kyrtsos, E. Skordis, C. T. Papadopoulos, R. Vlastou, A. Lagoyannis, and S. Andriamonje, Eur. Phys. J. A **49**, 62 (2013).
[3] C. Paradela *et al.*, Phys. Rev. C **82**, 034601 (2010).
[4] O. Shcherbakov *et al.*, J. Nucl. Sci. Tech. Suppl. **39**, 230 (2002).
[5] P. Cennini *et al.*, *Proceedings of the XII Intern. Seminar on Interaction of Neutrons with Nuclei*, No. 12 (J.I.N.R., Dubna, 2004), p. 456.
[6] K. Merla, P. Hausch, C. Herbach, G. Musiol, G. Pausch, U. Todt, L. Drapchinskiy, V. Kalinin, and V. Shpakov, *Proceedings of the International Conference on Nuclear Data for Science and Technology (1991)*, edited by R. Haight, M. Chadwick, T. Kawano, and P. Talou, Vol. 510 (American Institute of Physics, College Park, MD, 2005).
[7] P. Lisowski, J. Ullman, S. Balestrini, A. Carlson, O. Wasson, and N. Hill, *Conference on Nuclear Data for Science and Technology*, edited by S. Igarasi (Japan Atomic Energy Research Institute, Mito, Japan, 1988), p. 97.
[8] W. Jingxia, R.Chaofan, S. Zhongfa, L. Jingwen, Y. Zongyuan, and D. Xinlu, Chin. J. Nucl. Phys. **6**, 369 (1984).
[9] K. R. Zasadny, H. M. Agrawal, M. Mahdavi, and G. F. Knoll, Trans. Am. Nucl. Soc. **47**, 425 (1984).
[10] J. W. Meadows, Nucl. Sci. Eng. **85**, 271 (1983).
[11] M. Varnagy, S. Juhasz, and J. Csikai, Nucl. Instrum. Methods Phys. Res. **196**, 465 (1982).
[12] K. Kobayashi, I. Kimura, H. Gotoh, and H. Yagi, Tech. Rep. 6, Kyoto University, Research Reactor Institute, Kyoto, Japan (1973).
[13] R. Jiacoletti, W. Brown, and H. Olson, Nucl. Sci. Eng. **48**, 412 (1972).
[14] W. E. Stein, R. K. Smith, and H. L. Smith, Los Alamos Scientific Laboratory Tech. Rep. 9205, 1968 (unpublished).
[15] J. Grundl, Nucl. Sci. Eng. **30**, 30 (1967).
[16] P. H. White and G. P. Warner, J. Nucl. Energy **21** (1967).
[17] V. M. Pankratov *et al.*, At. Energ. **9**, 399 (1960).
[18] H. W. Schmitt and R. B. Murray, Phys. Rev. **116**, 1575 (1959).
[19] F. Tovesson and T. S. Hill, Phys. Rev. C **75**, 034610 (2007).
[20] K. Kanda, T. Iwasaki, M. Terayama, Y. Karino, M. Baba, and N. Hirakawa, Tohoku Univ., Dept. of Nucl. Engineering Reports, No. 47 (1986), Tohoku Univ., Sendai, Japan.
[21] A. A. Goverdovskii, A. K. Gordyushin, B. D. Kuzminov, V. F. Mitrofanov, A. I. Sergachev, S. M. Solovev, and G. M. Stepchenkova, Sov. At. Energy **58** (1985).
[22] J. W. Behrens, J. C. Browne, and J. C. Walden, Nucl. Sci. Eng. **80**, 393 (1982).
[23] M. B. Chadwick *et al.*, Nucl. Data Sheets **112**, 2887 (2011).
[24] K. Shibata and O. Iwamoto, *et al.*, J. Nucl. Sci. Technol. **48**, 1 (2011).
[25] JEFF-3.2, Evaluated Data Library (neutron data) OECD/NEA Data Bank Tech. Rep., 2014 (unpublished).
[26] Guo-Chang Chen *et al.*, Chin. Phys. C **36** (2012).
[27] RUSFOND-2010 Library, Institute of Physics and Power Engineering Tech. Rep., Obninsk, Russia, 2010 (unpublished).
[28] C. Rubbia *et al.*, A high resolution spallation driven facility at the CERN-PS to measure neutron cross-sections in the Interval from 1 eV to 250 MeV, CERN/LHC/98-02 (EET), CERN, 1998.
[29] M. Calviani *et al.*, Nucl. Instrum. Methods Phys. Res., Sect. A **594**, 220 (2008).
[30] EMPIRE-3.2 Malta, M. Herman *et al.*, INDC(NDS)-0603, BNL-101378-2013, Brookhaven National Laboratory, Upton, USA.
[31] n_TOF Collaboration, CERN/INTC-O-011, INTC-2002-037, Tech. Rep. CERN-SL-2002-053 ECT, 2003 (unpublished).
[32] C. Borcea *et al.*, Nucl. Instrum. Methods Phys. Res., Sect. A **513** (2003).
[33] U. Abbondanno *et al.*, Tech. Rep. CERN-SL-2002-053 ECT, 2003 (unpublished).
[34] M. Diakaki *et al.*, in *Proceedings of the 21st Symposium of the Hellenic Nuclear Physics Society* (N.C.S.R. Demokritos, Athens, Greece, 2012), pp. 81–88.
[35] M. Mayer, in *Proceedings of the 15th CAARI, AIP Conference Proceedings*, Vol. 475, edited by J. L. Duggan and I. L. Morgan (AIP, Denton Texas, USA, 1999), p. 541.
[36] D. Karadimos *et al.*, Nucl. Instrum. Methods Phys. Res., Sect. B **268**, 2556 (2010).
[37] D. Karadimos *et al.*, Phys. Rev. C **89**, 044606 (2014).

[38] F. James, *MINUIT: Function Minimization and Error Analysis Reference Manual (version 94.1)* (CERN, Geneva, Switzerland, 1998).
[39] A. Ferrari, P. Sala, A. Fasso, and J. Ranft, CERN-2005-10, INFN/TC_05/11, Tech. Rep. SLAC-R-773, 2005 (unpublished).
[40] G. D. Adeev, A. S. Botvina, A. S. Iljinov, M. V. Mebel, N. I. Poschasov, and O. I. Serdyuk, (1993), preprint, INR 816/93, Moscow.
[41] F.-J. Hambsch, F. Vives, P. Siegler, and S. Oberstedt, Nucl. Phys. A **679**, 3 (2000).
[42] C. A. Kalfas (private communication).
[43] J. Theuerkauf, S. Esser, S. Krink, M. Luig, N. Nicolay, O. Stuch, and H. Wolters, program TV, University of Cologne (unpublished).
[44] V. Vlachoudis, Beam Profile Calculator [http://pceet075.cern.ch].
[45] M. Herman, R. Capote, B. V. Carlson, B. Oblozinsky, M. Sin, A. Trkov, H. Wienke, and V. Zerkin, Nucl. Data Sheets **108**, 2655 (2007).
[46] M. Sin, P. Oblozinsky, M. Herman, and R. Capote, in *International Conference on Nuclear Data for Science and Technology 2007* (EDP sciences, Nice, France, 2007) [http://dx.doi.org/10.1051/ndata:07370].
[47] M. Sin, P. Oblozinsky, M. Herman, and R. Capote, J. Korean Phys. Soc. **59**, 1015 (2011).
[48] M. Sin, R. Capote, A. Ventura, M. Herman, and P. Oblozinsky, Phys. Rev. C **74**, 014608 (2006).
[49] M. Sin and R. Capote, Phys. Rev. C **77**, 054601 (2008).
[50] W. Hauser and H. Feshbach, Phys. Rev. **87**, 366 (1952).
[51] H. Hoffmann, J. Richert, J. Tepel, and H. Weidenmueller, Ann. Phys. (N.Y.) **90**, 403 (1975).
[52] R. Capote, S. Chiba, E. Sh. Soukhovitski, J. M. Quesada, and E. Bauge, J. Nucl. Sc. and Tech., **45**, 333 (2008).
[53] J. Raynal, IAEA Tech. Rep. No. SMR-9/8, 1972 (unpublished).
[54] A. D'Arrigo *et al.*, J. Phys. G **20**, 365 (1994).
[55] R. Capote, M. Herman, P. Oblozinsky *et al.*, Nucl. Data Sheets **110**, 3107 (2009).
[56] P. Sood, Z. Phys. A **318**, 111 (1984).